

Investigation of role of antisite disorder in the pristine cage compound FeGa_3

C. Kaufmann Ribeiro ¹, L. Mello ¹, V. Martelli¹, D. Cornejo ², M. B. Silva Neto ³, E. Fogh ⁴, H. M. Rønnow ⁴ and J. Larrea Jiménez ¹

¹ Laboratory for Quantum Matter under Extreme Conditions, Institute of Physics, University of São Paulo, São Paulo, Brazil

² Institute of Physics, University of São Paulo, São Paulo, SP, Brazil

³ Instituto de Física, Universidade Federal do Rio de Janeiro, Rio de Janeiro, Brazil

⁴ Laboratory for Quantum Magnetism, Institute of Physics, Ecole Polytechnique Fédérale de Lausanne (EPFL), Lausanne, Switzerland.

* larrea@if.usp.br

March 25, 2023

Abstract

The role of controlled Fe antisite disorder in the narrow gap semiconductor FeGa_3 has been investigated. Polycrystalline samples were synthesized by the combination of arc-melting furnace and successive annealing processes. Deviations from occupation numbers of Fe and Ga sites expected in the pristine compound were obtained from X-ray data using Rietveld refinement analysis. Besides that, electrical transport and magnetization measurements reveal that hierarchy in Fe and Ga site disorder tunes the ground state of FeGa_3 from paramagnetic semiconductor to a magnetic metal. These findings are discussed inside the framework of Anderson localization in the vicinity of metal-semiconductor transitions and spin fluctuations.

Contents

1 Introduction	2
2 Experimental	2
3 Results	3
4 Discussion	9
5 Conclusion	10
References	11

1 Introduction

Atomic disorder is an ubiquitous feature in realistic quantum materials. The presence of random defects, like vacancies, dislocations and impurities, induced during sample preparation is usually seen as an unfavorable mechanism to stabilize novel quantum states driven by quantum phase transitions [1]. However, a controlled modification of disorder can be used as tuning control parameter to investigate emergent quantum phenomena that go beyond the scope of decoherence and localization of fermions inducing Anderson-localized states [2]. This is the case, for instance, of antisite disorder in double perovskites and low-dimensional oxides compounds, where exotic magnetic and electronic states emerge [3, 4]. Last but not least, the investigation of the influence of antisite disorder on the correlation between electron and spin degrees of freedom is timely to establish alternative routes to uncover new quantum states of matter from a perspective of non-canonical quantum phase diagrams.

Considering the existing variety of synthetic crystal symmetries, compounds with cage-like structure offer fashionable platforms to investigate diverse problems in quantum materials, such as, collective spin and orbital states close to a quantum critical point (QCP) [5], anomalous electron-electron scattering process [6] and the interplay between magnetic frustration and disorder to stabilize spin glass phases [7].

Among cage-compounds, FeGa₃ is a strongly correlated narrow-gap semiconductor candidate and has been widely studied because of its unconventional magnetic and electronic properties that leads as a promising thermoelectric material [8–12]. Electrical resistivity measurements show an intrinsic activation gap ≈ 0.4 eV and indicate the presence of in-gap donor states just below the conduction band in pristine single-crystals [13, 14]. Although FeGa₃ has been widely accepted as a semiconductor, the inclusion of subtle amount of disorder might drive FeGa₃ to *p*-type metal [15]. Magnetic susceptibility and Mössbauer spectroscopy confirms the absence of long range magnetic interaction in pristine FeGa₃ [14, 16], in agreement with Density-Functional Theory (DFT) calculation [17]; while, neutron scattering shows signatures of a magnetic ground state, interpreted as a complex antiferromagnetic structure [18]. In addition, the chemical doping substitution of Ge atoms in Ga sites in the solid solution FeGa_{3-x}Ge_x induces a transition from a diamagnetic semiconductor to a ferromagnetic metal, with a putative QCP at $x_c \approx 0.14$. The coexistence between long-range and short-range magnetic order above x_c suggests that disorder induced by random Ge substitution plays an important role in the zero-temperature phase transition and its concomitant magnetic ground states [19]. More recently, first-principle electronic band calculations propose that a complex structure of metallic in-gap states driven by subtle Fe disorder might be responsible for the origin of very tiny magnetic moments likely interacting as a ferromagnetic ground state [20, 21].

Here, we present a study of the influence of Fe antisite disorder in the electronic and magnetic physical properties of FeGa₃ polycrystals. Our results show that the amount of Fe antisite disorder can be controlled optimizing the annealing process, which turns out in the inclusion of tiny excess of Fe atoms in one of the non-equivalent Ga atomic sites.

2 Experimental

Polycrystalline samples with Fe antisite disorder named as Fe_{1+ δ} Ga₃ (with nominal $\delta = 0.04$) was prepared by solid-state reaction using an arc-melt furnace with a successive annealing process. High purity Ga and Fe pallets were melted in a cold water-cooled copper crucible under an argon atmosphere at ambient pressure. The as-cast samples were ground in an agate mortar, and the powder subsequently homogenized in size. For the annealing, the samples were encapsulated in a quartz tube under vacuum $\approx 10^{-5}$ mTorr, treated at different annealing

temperature T_a for 24h, and cooled down to ambient temperature at a rate of 0.4 °C/min.

XRD diffraction were collected with a Diffractometer Rigaku Ultima III with angular step of 0.02° and $K\alpha$ -Cu wavelength. Energy dispersive x-ray spectroscopy (EDS) confirms the expected δ off-stoichiometric revealed by our Rietveld refinement analysis of XRD data within 5 % of uncertainty. Magnetization is measured at ambient temperature using a vibrating-sample-magnetometer (VSM) and DC magnetic field up to 1.5 T. For electrical transport measurements samples were compressed in circular pellets of 3 mm in diameter. Electrical resistivity (ρ) is measured in Van-der-Pauw configuration down to 16 K.

3 Results

Figure 1 shows the XRD patterns of the powdered samples at different annealing temperatures, T_a . The $P4_2/mnm$ space group symmetry of the $FeGa_3$ phase is confirmed by Rietveld refinement (RR) for all T_a . No spurious phase is observed in the resolution of our XRD instrumentation. The lattice parameters in the as-cast sample $a = 6.2645(4)$ Å and $c = 6.5568(7)$ Å are in agreement with those values reported in literature for single-crystals [21]. Under annealing we did not observed significant change in the lattice parameter.

Our starting approach considers that the $P4_2/mnm$ space group symmetry arranges Fe and Ga atoms at three inequivalent Wyckoff sites $4f$, $8j$ and $4c$ [18]. In the case of the pristine compound $FeGa_3$, the disorder is not takes into account leading to $4f$ sites to be fully occupied by Fe atoms, whereas $8j$ and $4c$ sites host two inequivalent Ga atoms. On the other hand, when antisite disorder is considered, there are two possible arrangements : either Fe atoms might also occupy the $8j$ and $4c$ sites or the two inequivalent Ga sites extent their occupation at the $4f$ sites. If the former scenario sets in then Fe antisite disorder is formed and accounts for the tiny excess of Fe content in proportion to the pristine compound $FeGa_3$.

In order to evaluate the presence of antisite disorder, we compute the crystal structure of $FeGa_3$ using a careful RR analysis of our XRD data. Special attention is paid to the site occupancy number (SON) obtained in our RR results. Because SON is defined as the chemical occupancy times site multiplicity and normalized to the multiplicity of the general position, then the occupancy number and its influence in the quality of the RR-XRD patterns dictate which is the most appropriate atomic arrangement inside the primitive cell. By comparison of all the three different input RR patterns, i.e; non-disordered pristine compound, Ga antisite disorder and Fe antisite disorder, the latter gives a most accurate description of our experimental data for all samples at different conditions of synthesis (see Fig. 1). Besides, due to our good quality XRD data, we used the Bragg R-factor ($|R_B|$) as another indicator to validate our initial proposed model including Fe antisite disorder. Because $|R_B|$ compares the observed and calculated integrated intensity (the latter also connected with the structural factor) [22], we found the lowest $|R_B|$ values (see table 1) when Fe antisite disorder is included at the wickoff position $8j$ and $4c$.

Fig. 2 depicts the variation of the occupancy number as function of the annealing temperature and compares with as-cast sample. The reduction of the SON with the annealing temperature up to $T_a \approx 600$ °C indicates that Fe antisite disorder reaches a stable quantity nearly above this temperature. It is also remarkable that Fe antisite disorder prefers to displace Ga atoms mainly at the $8j$ sites.

Another evidence of the presence of Fe antisite disorder can be inferred from the computation of the q -vector dependence of the structure factor $S(q)$ [23] :

$$S(Q) = \sum_{n=1}^n O_{Ga}^n f_{Ga}(Q) e^{-2\pi i(h\mu_n + kv_n + lw_n)} + O_{Fe}^n f_{Fe}(Q) e^{-2\pi i(h\mu_n + kv_n + lw_j)} \quad (1)$$

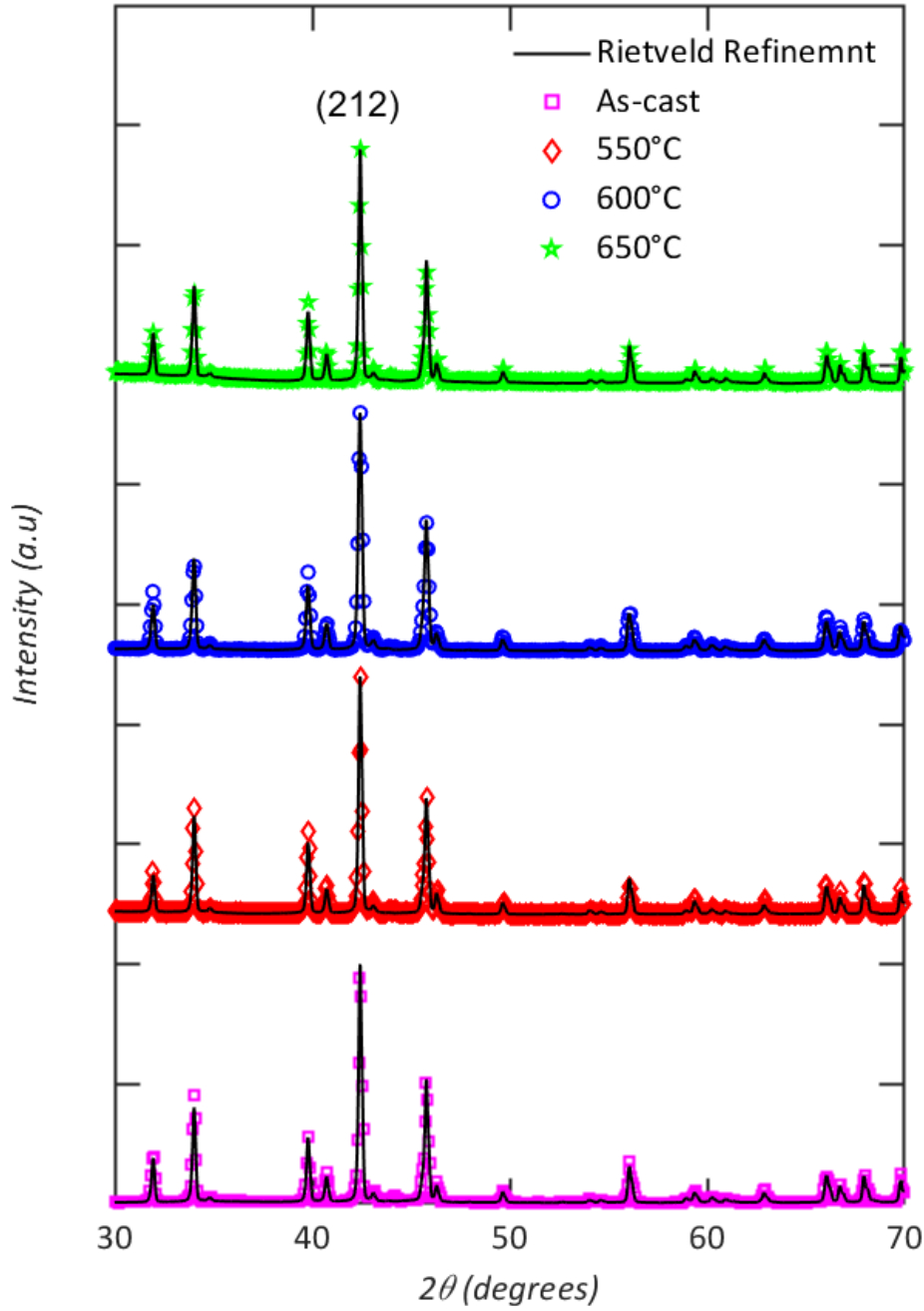


Figure 1: Experimental (open points) and calculated (black line) XRD patterns of as-cast and annealed FeGa₃ polycrystals.

Where $O_{Ga,Fe}$ and $f_{Ga,Fe}(Q)$ represent the atomic occupancy and the atomic form factor of Ga and Fe atoms, respectively. The terms in the imaginary exponential are the fractional position of n th-atomic site in the primitive unit cell (u_n, v_n, w_n) and the reflection plane index (h, k, l). The summation extends over all different atomic species at different sites in the primitive lattice. Given the Gaussian interpolation methods [24] we inferred the $f_{Ga}(Q)$ and $f_{Fe}(Q)$ values. The other parameters are quoted from symmetry operations of the $P4_2/mnm$

space group for the inequivalent sites $8j$, $4c$ and $4f$ as it is the case of (u_n, v_n, w_n) , as well as, from analogue equivalence between occupancy number in our RR analysis and those atomic occupancy to be used in eq. 1. Starting from the pristine compound FeGa_3 , we use those values expected for single crystal [18], i.e. $O_{Ga}^{8j} = O_{Ga}^{4c} = 1$ for Ga atoms at site $8j$ and $4c$ while $O_{Fe}^{4f} = 1$ for Fe atoms at site $4f$. Thus $O_{Ga} = O_{Fe} = 0$ if Ga and Fe atoms occupy different Wyckoff sites. In contrast when Fe antisite disorder takes place, $O_{Fe}^{4f} = 1$ and $0 \leq O_{Fe}^{4c}, O_{Fe}^{8j} \leq 1$ constraining the Ga occupancy $O_{Ga}^n = 1 - O_{Fe}^n$ for any Wyckoff site. After a proper comparative normalization of SON values (see fig. 2), obtained from our RR analysis we include the atomic occupancy of Ga and Fe and determine the structure factor at different annealing conditions. $S(Q)$ for pristine FeGa_3 in the presence of Fe antisite disorder for as-cast and annealed samples are depicted in figure 3. As we can observe in fig. 3, oscillatory deviations from that $S(Q)$ expected for the pristine compound become less pronounced with the increasing of annealing temperature, at least up to 650°C . Together with the variation of the occupancy number (see fig. 2) both SON and $S(Q)$ features that the Fe antisite disorder is controlled by annealing temperature until Fe atoms displace completely the Ga counterpart at $8j$ site.

Table 1: Bragg R-factor ($|R_B|$) from RR with and without inclusion of Fe antisite disorder

	As-cast	550°C	600°C	650°C
Without Fe antisite	7.36%	10.23%	9.89%	13.37%
With Fe antisite	6.92%	9.7%	9.57%	13.27%

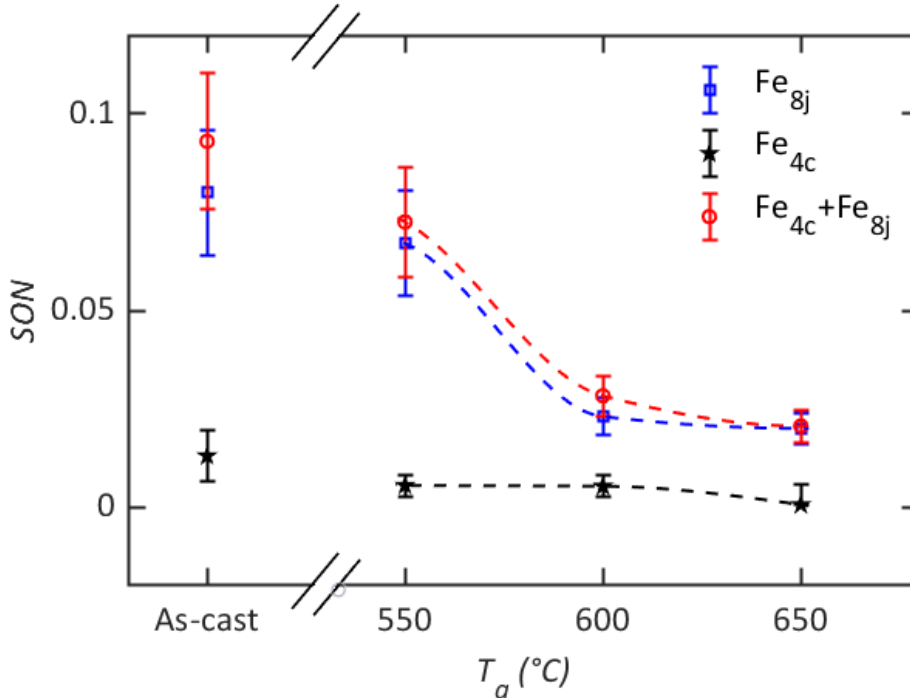


Figure 2: Site occupation number (SON) of Fe antisite as function of annealing temperature T_a and compared with SON for as-cast sample. Fe atoms can occupy different non-equivalent crystallographic sites. The dashed lines are guide for the eyes.

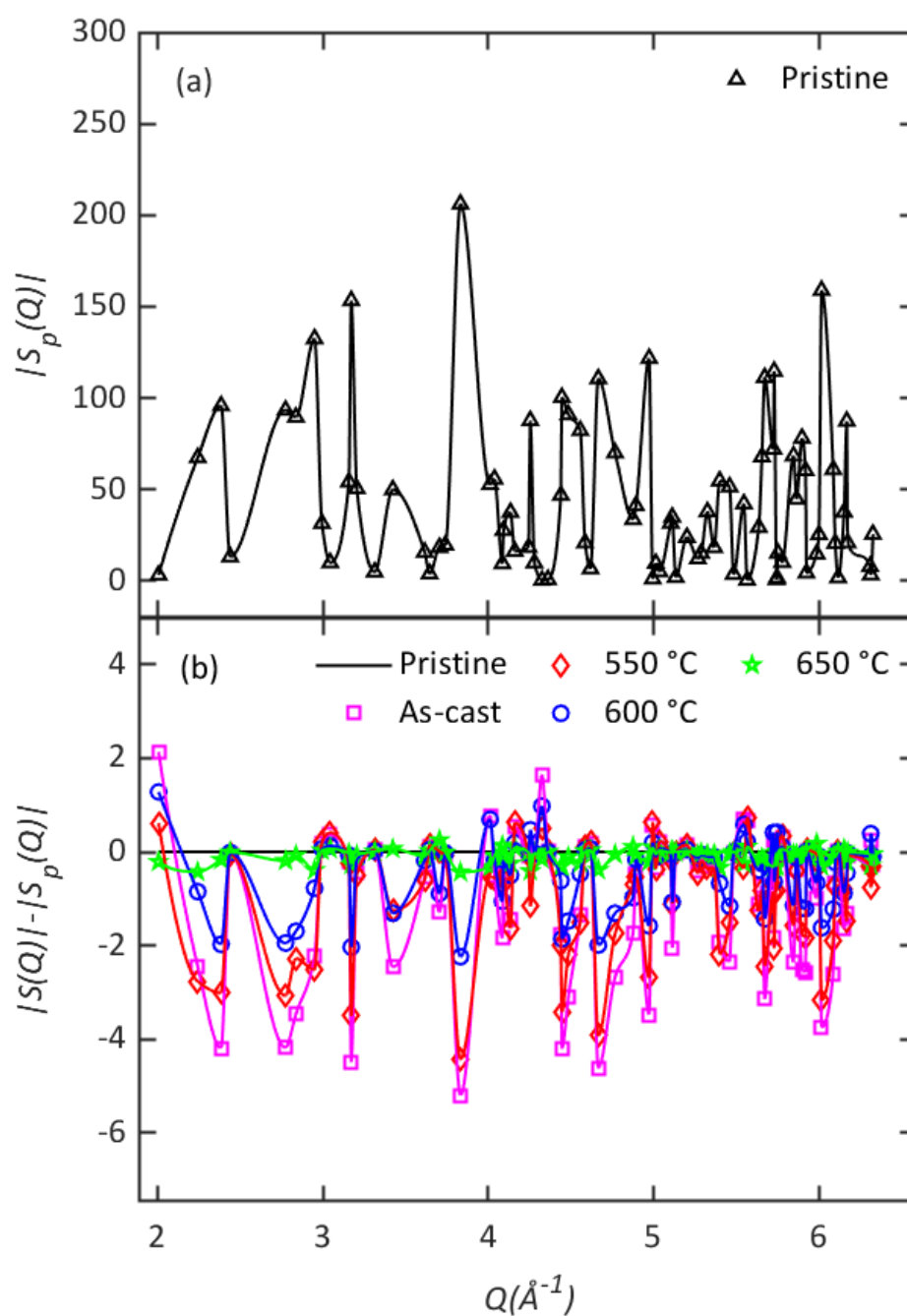


Figure 3: (a) Structural factor for the pristine FeGa_3 sample (b) Difference between the structural factor $S(q)$ for FeGa_3 polycrystalline samples annealed with different temperatures with respect to the structure factor expected for the pristine FeGa_3 polycrystal, $S_p(q)$. The continuous black line evaluates $S_p(q) - S_p(q)$.

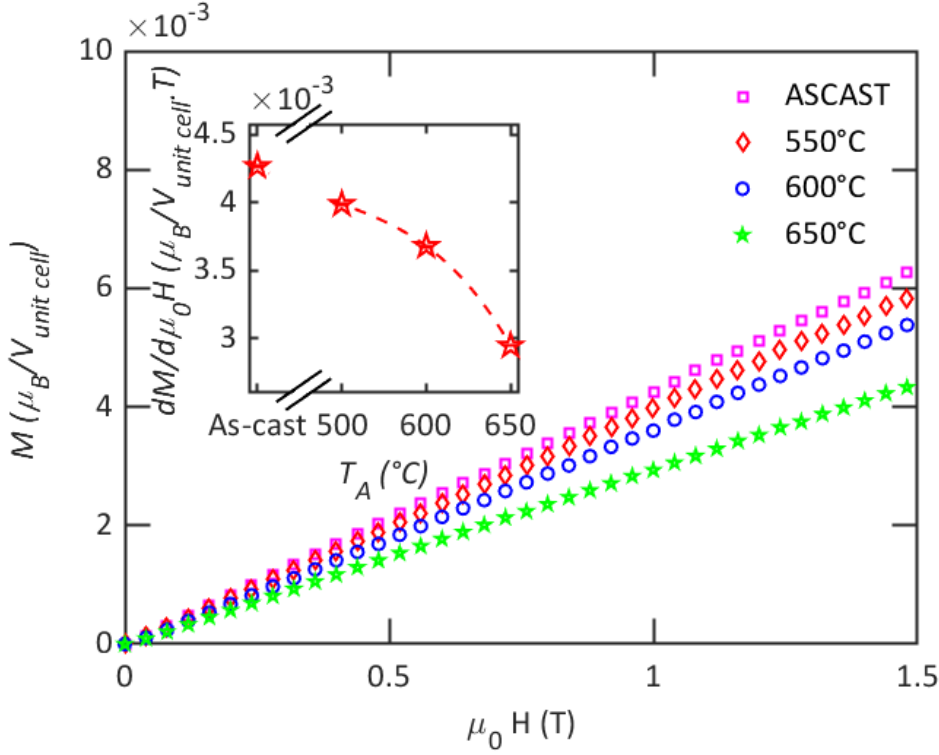


Figure 4: Field dependence of the magnetization per unit cell volume given at room temperature (295 K) for different annealing temperatures. The inset shows the annealing temperature dependence of the magnetic susceptibility at ambient temperature.

On the other hand, the linear field dependence of the magnetization (M) per unit cell volume ($V_{\text{unit cell}}$), shown in 4, reveals a paramagnetic behavior in the presence of antisite disorder at room temperature (295 K). The increase of T_a reduces the magnetic susceptibility $\frac{dM}{d\mu_0 H}$ in the samples, which might indicate a reduction of diluted magnetic moments if they likely formed under the influence of Fe antisite disorder.

Other features about the role of Fe antisite disorder can be inferred from the temperature dependence of the electrical transport $\rho(T)$ shown in figure 5. Starting from the as-cast specimen, $\rho(T)$ shows a metallic behavior. The electrical resistivity (see figure 5) shows that the annealing induces significant changes in the electronic states mainly below 200 K. Successive annealing induces an upturn on $\rho(T)$ at $T \approx 200\text{K}$, which is attributed to a semiconducting extrinsic response due to in-gap donor states. The metal-semiconductor transition is likely related to the fact that the annealing decreases the concentration of Fe antisite. The Arrhenius law can well describe the electrical resistivity of the annealed samples, $\rho \propto e^{E_g/2k_b T}$, in the range of 100 K-160 K (see figure 5 (b)), where E_g is the energy separation from in-gap donor states to the conduction band. On the contrary for the as-cast sample, the metallic behavior allows to describe $\rho(T) \propto A_f T^2$ (figure 5 (c)) resulting with a quadratic coefficient $A_f \approx 0.38(2) \mu\Omega\text{cm}/\text{K}^2$.

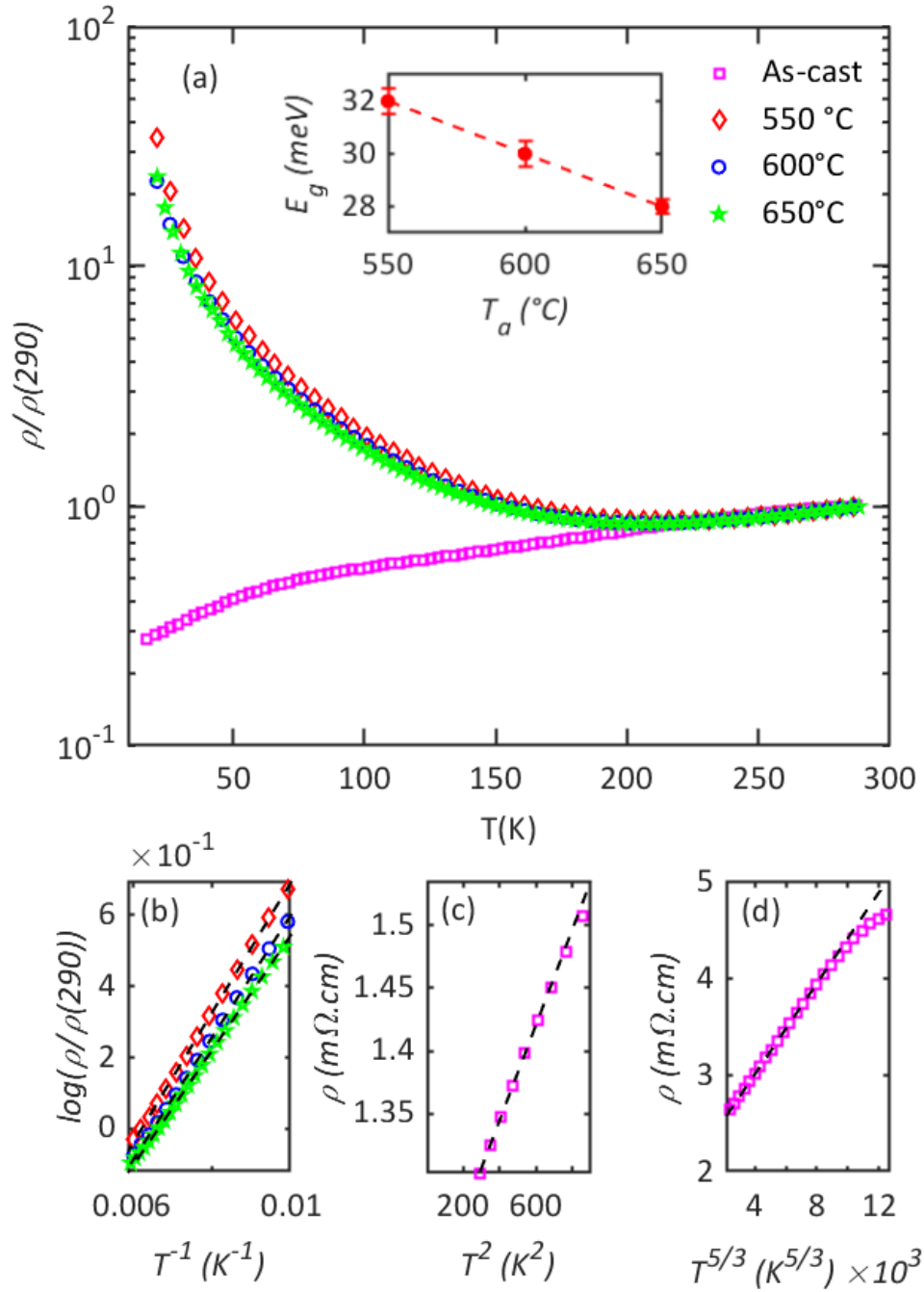


Figure 5: Figure (a): Temperature dependence of normalized electrical resistivity of FeGa₃ annealed at different T_a . The inset shows the temperature dependence of the energy gap from the in-gap donor state to the conduction band, lines are guide for the eyes. Figure (b): Arrhenius plot at 100 K to 160 K temperature range for the annealed samples. Figure (c): Low temperature T^2 -dependence of electrical resistivity of as-cast sample. Figure (d): Comparison with $T^{5/3}$ dependence of electrical resistivity of as-cast sample .

4 Discussion

Recent Density Functional Theory (DFT) calculations have reported the influence of intrinsic disorder in FeGa_3 on the formation of in-gap states and diluted magnetic moments [20]. In addition, low-temperature magnetization measurements have shown the development of ferromagnetic ordering for non-stoichiometric Fe-rich FeGa_3 single crystals where the formation of this magnetic state was addressed to disorder-induced in-gap metallic states [21]. Previous electrical transport and spin-lattice relaxation experiments have indicated the presence of magnetic in-gap states intrinsic to FeGa_3 [25]. However, in all these previous results where disorder influences the pristine ground state in FeGa_3 , there is an absence of investigation if disorder arises from antisite or random configuration of atoms.

In the present study XRD, indicates that the density of antisite Fe defects decreases with annealing temperature, and induces a reduction of in-gap states near the Fermi energy, as well as the decrease of the magnetic susceptibility at ambient temperature.

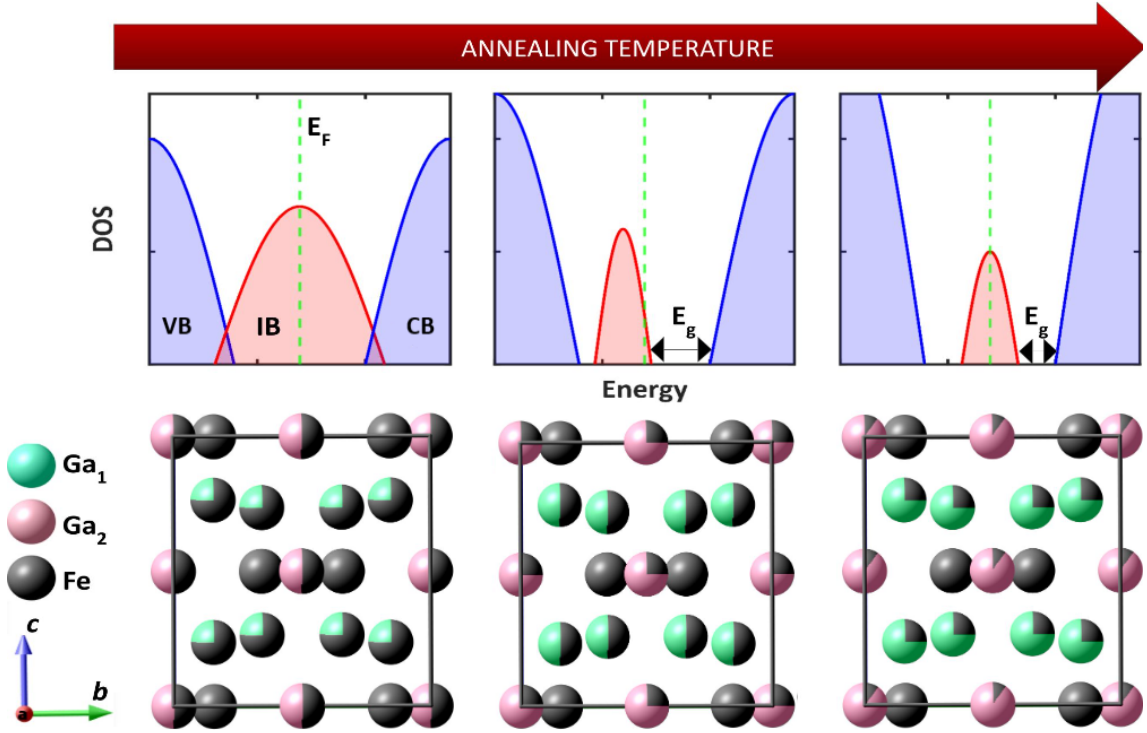


Figure 6: Schematic representation of electronic band (upper) and unit cell (lower) of $\text{Fe}_{1+\delta}\text{Ga}_3$ as function of annealing temperature. CB = conduction band, VB = valence band, IB = intermediate in-gap band and E_g is the extrinsic gap, that decreases with the annealing temperature. The semi-filled spheres represents the amount of Fe antisite disorder at the Ga positions.

The scenario of in-gap states can also be used to explain the metal-semiconductor transition observed in our investigation. The observed $\rho(T)$ with E_g at some decades of meV might indicate a type of metal-semiconductor Anderson transition, which occurs when the number of defects on the sample increases to a critical concentration called the percolation threshold. Below the critical concentration of defects, the in-gap states are localized due to the Anderson-localization effect [2]. On the other hand, as discussed by Mott, as the number of impurities approaches the critical concentration, the mobility edges shift towards the band edges and above a critical point, all the impurity states become delocalized, inducing a metallic behavior in the system [26]. Therefore, as the annealing temperature increases and the number of

Fe-based defects are reduced, the band-edges of the impurity band (IB) shrink, separating the localized in-gap states from the delocalized extended states driving IB within the semiconductor intrinsic gap (see E_g in figure 6). From our $\rho(T)$, we estimated the impurity activation gap (E_g) (plotted in the inset of figure 5 (a)). The decrease of E_g with the annealing temperature before $\text{Fe}_{1+\delta}\text{Ga}_3$ amorphized suggests that the localized impurity states go towards the conduction band while its bandwidth is reduced, as result of the decrease of localized impurity concentration.

On the other hand, the high concentration of defects in the as-cast sample, the delocalization of the in-gap states, gives rise to a metallic behavior. The Fermi-liquid behavior found in $\rho(T)$ as-cast sample reminisces of a problem involving defect-induced dirty metal, for which the additional free carriers induced by disorder contributes to the increase of paramagnetic susceptibility and enhancement of the momentum relaxation [27]. However, the large value of the quadratic coefficient in the FL-fitting (see fig. 5 (c)) $A_f \approx 0.38(2)\mu\Omega\text{cm}/\text{K}^2$ can not exclude the scenario of a strong renormalization in the effective mass likely induced by the presence of strong electronic correlations or spin fluctuations. In addition the $T^{5/3}$ dependence of the ρ in a wide range of temperatures, within 90-230 K (see Fig. 5 (d)) might indicate followed by slow saturation, indicates the presence of spin fluctuations, which could also cause the renormalization of the quadratic coefficient at low temperatures. Spin fluctuations are also observed in the metallic-ferromagnetic phase of $\text{FeGa}_{3-x}\text{Ge}_x$ to high dopant concentration and mediate marginal Fermi-liquid state on the border of ferromagnetism near the critical point [19]. The presence of spin fluctuations induced by strong antisite disorder in our as-cast samples recalls the scenario that spin dynamics might play a relevant role in the quantum critical behavior and non-canonical quantum critical material phase of $\text{FeGa}_{3-x}\text{Ge}_x$ system, which is tuned to a putative FM-QPC by random substitution of Ge [19]. Our findings trigger future low-temperature investigation of the magnetic properties of $\text{Fe}_{1+\delta}\text{Ga}_3$ to reveal the nature of the magnetic ground state competing with spin fluctuations mechanism in a system with antisite disorder features.

5 Conclusion

The effect of controlled antisite disorder in FeGa_3 on the electronic, magnetic and crystallographic structure has been studied in polycrystalline $\text{Fe}_{1+\delta}\text{Ga}_3$ samples with a slight excess of Fe identified as Fe antisite disorder.

Fe-defects induce paramagnetic and metallic states at ambient temperature. Tiny decrease of impurities induced by annealing reduces the magnetic susceptibility and changes the ground state from a disordered correlated metal to a magnetic narrow-gap semiconductor. The later is possibly due to the transition of a delocalized impurity band to localized in-gap states as the number of defects approaches the percolation threshold. These findings contribute to a better understanding of the role of disorder in FeGa_3 and motivates further studies of the nature of the disordered-driven semiconductor-metal transition in FeGa_3 and the role of spin-fluctuation and strong correlations.

Acknowledgements

Funding information JLJ acknowledges support of JP-FAPESP (2018/08845-3) and CNPq-PQ2 (310065/2021-6), C.K.R acknowledges the support of FAPESP (2019/24522-2), VM acknowledges the support of JP-FAPESP (2018/19420-3). We acknowledge M.C.A. Fantini for the access to the LCr-IFUSP

References

- [1] T. Vojta, Annual Review of Condensed Matter Physics **10**(1), 233 (2019).
- [2] P. W. Anderson, Phys. Rev. **109**, 1492 (1958).
- [3] W. Li, J. Shi, K. H. Zhang and J. L. MacManus-Driscoll, Materials Horizons **7**(11), 2832 (2020).
- [4] E. E. Ateia, A. T. Mohamed and H. Elshimy, Applied Nanoscience **10**(5), 1489 (2020).
- [5] V. Martelli, A. Cai, E. M. Nica, M. Taupin, A. Prokofiev, C.-C. Liu, H.-H. Lai, R. Yu, K. Ingersent, R. K uchler *et al.*, *Sequential localization of a complex electron fluid*, Proceedings of the National Academy of Sciences **116**(36), 17701 (2019).
- [6] F. Han, J.-K. Bao, C. D. Malliakas, M. Sturza, Y. Du, D. Y. Chung, X. Wan and M. G. Kanatzidis, *Enormous electron-electron scattering in the filled-cage cubic compound $b a 10 t i 24 b i 39$* , Physical Review Materials **3**(10), 105001 (2019).
- [7] V. M. Katukuri, S. Nishimoto, I. Rousochatzakis, H. Stoll, J. Van Den Brink and L. Hozoi, *Strong magnetic frustration and anti-site disorder causing spin-glass behavior in honeycomb $li2rho3$* , Scientific reports **5**(1), 1 (2015).
- [8] N. Haldolaarachchige, A. Karki, W. A. Phelan, Y. Xiong, R. Jin, J. Y. Chan, S. Stadler and D. Young, Journal of Applied Physics **109**(10), 103712 (2011).
- [9] Y. Takagiwa, Y. Matsuura and K. Kimura, Journal of electronic materials **43**(6), 2206 (2014).
- [10] M. Wagner-Reetz, R. Cardoso-Gil and Y. Grin, Journal of electronic materials **43**(6), 1857 (2014).
- [11] V. Ponnambalam and D. T. Morelli, Journal of Applied Physics **118**(24), 245101 (2015).
- [12] J. Alvarez-Quiceno, G. Dalpian, A. Fazzio and J. Osorio-Guill en, Journal of Physics: Condensed Matter **30**(8), 085701 (2018).
- [13] U. H ussermann, M. Bostr om, P. Viklund,  . Rapp and T. Bj rn ngen, Journal of Solid State Chemistry **165**(1), 94 (2002).
- [14] Y. Hadano, S. Narazu, M. A. Avila, T. Onimaru and T. Takabatake, Journal of the Physical Society of Japan **78**(1), 013702 (2008).
- [15] C.-S. Lue, W. Lai and Y.-K. Kuo, Journal of alloys and compounds **392**(1-2), 72 (2005).
- [16] N. Tsujii, H. Yamaoka, M. Matsunami, R. Eguchi, Y. Ishida, Y. Senba, H. Ohashi, S. Shin, T. Furubayashi, H. Abe *et al.*, Journal of the Physical Society of Japan **77**(2), 024705 (2008).
- [17] J. M. Osorio-Guill en, Y. D. Larrauri-Pizarro and G. M. Dalpian, Physical Review B **86**(23), 235202 (2012).
- [18] M. Gam za, J. Tomczak, C. Brown, A. Puri, G. Kotliar and M. Aronson, Physical Review B **89**(19), 195102 (2014).
- [19] J. Munevar, M. Cabrera-Baez, M. Alzamora, J. Larrea, E. M. Bittar, E. Baggio-Saitovitch, F. J. Litterst, R. A. Ribeiro, M. A. Avila and E. Morenzoni, Phys. Rev. B **95**, 125138 (2017).

- [20] J. C. Alvarez-Quiceno, M. A. Avila, J. M. Osorio-Guillén and G. M. Dalpian, *Phys. Rev. B* **102**, 094110 (2020).
- [21] F. R. Wagner, R. Cardoso-Gil, B. Boucher, M. Wagner-Reetz, J. Sichelschmidt, P. Gille, M. Baenitz and Y. Grin, *Inorganic chemistry* **57**(20), 12908 (2018).
- [22] B. H. Toby, *R factors in rietveld analysis: How good is good enough?*, *Powder diffraction* **21**(1), 67 (2006).
- [23] Y. Waseda, E. Matsubara and K. Shinoda, *X-ray diffraction crystallography: introduction, examples and solved problems*, Springer Science & Business Media (2011).
- [24] E. Prince and P. Boggs, *International tables for crystallography (2006). vol. c, chapter 8.1*, pp. 678–688. (2006).
- [25] A. Gippius, V. Y. Verchenko, A. Tkachev, N. Gervits, C. Lue, A. Tsirlin, N. Büttgen, W. Krätschmer, M. Baenitz, M. Shatruk *et al.*, *Physical Review B* **89**(10), 104426 (2014).
- [26] N. F. Mott, *Reviews of Modern Physics* **40**(4), 677 (1968).
- [27] S. M. Girvin and K. Yang, *Modern condensed matter physics*, Cambridge University Press (2019).